PNAS
www.pnas.org

SI Appendix

Evidence for high-density liquid water between 0.1 and 0.3 GPa near 150 K

Josef N. Stern[†], Markus Seidl-Nigsch[†‡] and Thomas Loerting[†*]

[†] Institute of Physical Chemistry, University of Innsbruck, A-6020 Innsbruck, Austria

[‡] Current Address: Materials Development, Getzner Werkstoffe GmbH, Herrenau 5, 6706 Bürs, Austria

[*]Correspondence and requests for materials should be addressed to T.L. (email: thomas.loerting@uibk.ac.at)

This PDF file includes:

Supplementary Text

Figures S1 to S5

Tables S1 to S5

References for SI reference citations

www.pnas.org/cgi/doi/10.1073/pnas.1819832116

Bragg peaks of crystalline ices

Table S1: Most intense crystalline ice Bragg peaks (100 % relative intensity).

Crystalline phases	Ice I Ref. (1)	Ice II Ref. (2)	Ice IV Ref. (3)	Ice V Ref. (4)	Ice VI Ref. (5)	Ice IX Ref. (6)	Ice XII Ref. (7)
Most intense Bragg peak (2θ[°])	24.2	29.6	31.6	33.8	35.5	29.8	32.8

Crystallization temperatures T_x

In Figure S1 the crystallization temperatures determined as illustrated in Figure S4 are plotted against the pressure. The values of T_x are listed in Table S2 and are used to define the lines of crystallization $T_x(p)$ displayed in Figure 1.

Table S2: Pressure dependence of the onset crystallization temperatures T_x of the five amorphous samples. Literature values (8, 9) in case of uHDA and $eHDA^{0.2}_{1.1}$ are marked with an asterisk (*).

	T_x(uHDA)	$T_x(eHDA^{0.2}_{1.1})$	$T_x(eHDA^{0.2}_{1.9})$	$T_x(VHDA_{1.1})$	$T_x(VHDA_{1.9})$
0.1 GPa	133.5 K *	144.0 K *	142.8 K	–	143.9 K
0.2 GPa	142.5 K *	149.5 K *	148.5 K	–	149.0 K
0.3 GPa	148.5 K *	154.0 K *	153.8 K	–	154.1 K
0.4 GPa	151.5 K *	156.5 K *	155.4 K	–	157.8 K
0.5 GPa	155.0 K *	158.5 K *	158.1 K	–	161.6 K
0.6 GPa	155.6 K	160.3 K	160.6 K	161.7 K	162.7 K
0.7 GPa	156.9 K	161.6 K	162.4 K	163.5 K	164.1 K
0.8 GPa	161.5 K	163.1 K	164.7 K	165.4 K	166.5 K
0.9 GPa	164.1 K	165.1 K	165.6 K	166.2 K	169.2 K
1.0 GPa	165.0 K	165.8 K	–	168.7 K	171.4 K
1.1 GPa	167.5 K	166.9 K	–	169.5 K	172.5 K
1.3 GPa	171.6 K	169.4 K	170.3 K	171.0 K	176.1 K
1.6 GPa	175.1 K	174.0 K	174.6 K	174.6 K	179.2 K
1.8 GPa	178.9 K	177.2 K	176.6 K	177.2 K	184.0 K
1.9 GPa	177.1 K	175.9 K	174.0 K	178.1 K	178.9 K

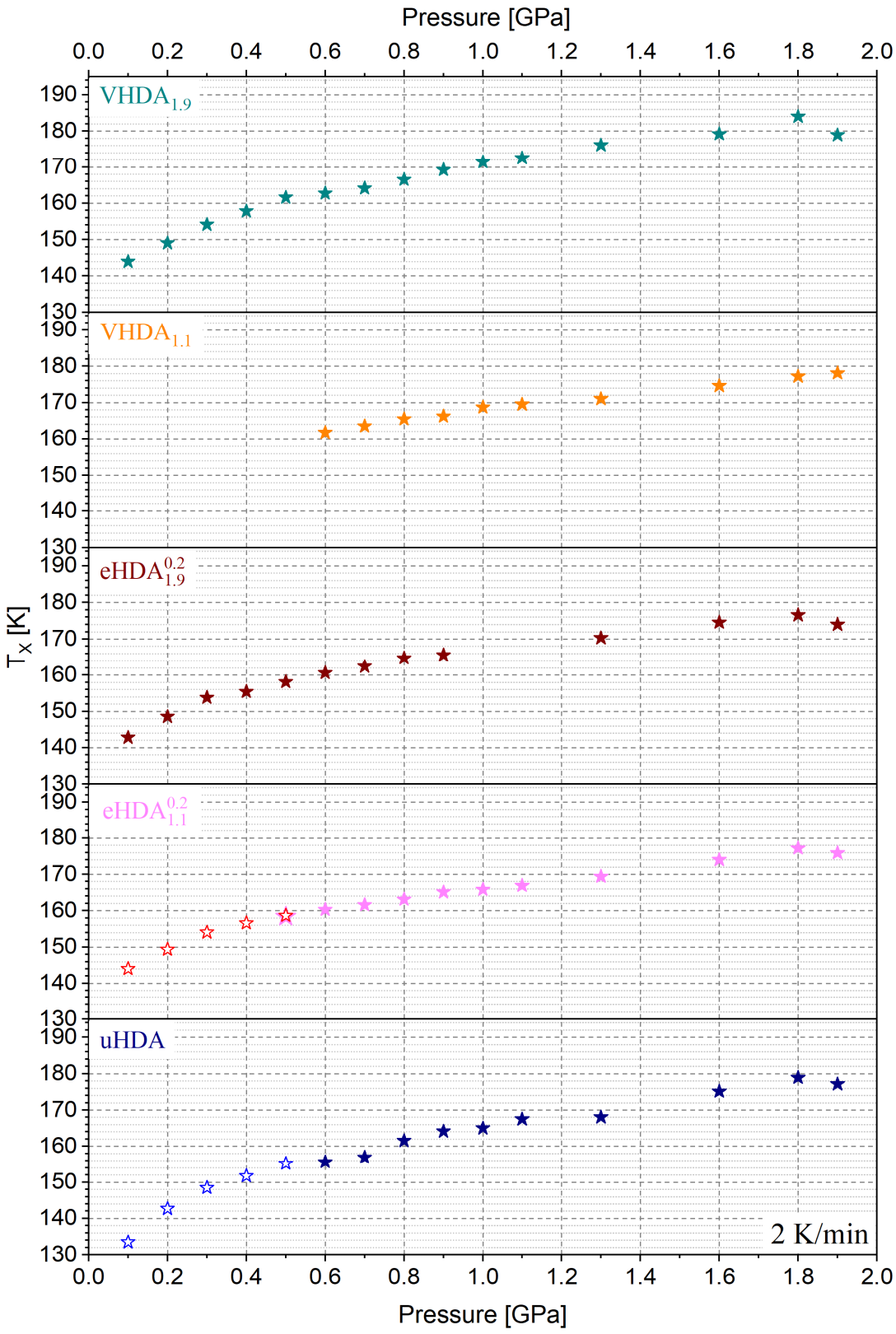

Figure S1: Crystallization temperatures T_x against pressure. All samples were heated isobarically with a rate of 2 K/min. Values of T_x were evaluated as demonstrated in Figure S4. The open star symbols in case of $eHDA^{0.2}_{1.1}$ (red) and uHDA (blue) are literature values from References (8) and (9).

The structural data that is displayed in Figure 5 is listed numerically in Table S3.

Table S3: Crystalline phase compositions of the amorphous ices at the respective pressures. Values were determined by comparing the most intense crystalline ice phase (see Table S1) in a given mixture. The data represent a tabular form of Figure 5.

	uHDA			eHDA$^{0.2}_{1.1}$			eHDA$^{0.2}_{1.9}$			VHDA$_{1.1}$			VHDA$_{1.9}$		
0.1 GPa	~ 90 % (I)	~ 10 % (IX)		~ 90 % (I)	~ 10 % (IX)		60 % (I)	40 % (IX)		-			68 % (I)	32 % (IX)	
0.2 GPa	~ 60 % (I)	~ 40 % (IX)		100 % (IX)			99 % (IX)	1 % (V)		-			100 % (IX)		
0.3 GPa	~ 99 % (IX)	~ 1 % (V)		~ 90 % (IX)	~ 10 % (V)		95 % (IX)	5 % (V)		-			99 % (IX)	1 % (V)	
0.4 GPa	100 % (IX)			~ 95 % (IX)	~ 5 % (V)		57 % (IX)	43 % (V)		100 % (V)			49 % (IX)	51 % (V)	
0.5 GPa	~ 99 % (IX)	~ 1 % (V)		35 % (IX)	63 % (V)	2 % (IV)	29 % (IX)	52 % (V)	2 % (IV)	17 % (XII)	8 % (II)	70 % (IX)	22 % (V)	12 % (IX)	14 % (V)	16 % (IV)	58 % (XII)
0.6 GPa	34 % (V)	66 % (IV)		4 % (IX)	7 % (V)	7 % (IV)	82 % (XII)	2 % (IX)	10 % (V)	2 % (IV)	86 % (XII)	62 % (IX)	28 % (V)	9 % (IV)	1 % (XII)	1 % (V)	3 % (IV)	96 % (XII)
0.7 GPa	33 % (V)	67 % (IV)		4 % (V)	10 % (IV)	86 % (XII)	16 % (IV)	84 % (XII)		21 % (IV)	79 % (XII)		5 % (IV)	95 % (XII)	
0.8 GPa	33 % (IV)	67 % (XII)		20 % (IV)	80 % (XII)		16 % (IV)	84 % (XII)		6 % (IV)	94 % (XII)		2 % (IV)	98 % (XII)	
0.9 GPa	9 % (IV)	91 % (XII)		6 % (IV)	94 % (XII)		5 % (IV)	95 % (XII)		15 % (IV)	85 % (XII)		6 % (IV)	94 % (XII)	
1.0 GPa	3 % (IV)	97 % (XII)		6 % (IV)	94 % (XII)		-			13 % (IV)	87 % (XII)		81 % (XII)	19 % (VI)	
1.1 GPa	11 % (IV)	89 % (XII)		5 % (IV)	95 % (XII)		-			4 % (IV)	96 % (XII)		90 % (XII)	10 % (VI)	
1.3 GPa	5 % (IV)	90 % (XII)	5 % (VI)	4 % (IV)	92 % (XII)	4 % (VI)	2 % (IV)	88 % (XII)	10 % (VI)	5 % (IV)	92 % (XII)	3 % (VI)	73 % (XII)	27 % (VI)	
1.6 GPa	83 % (XII)	17 % (VI)		4 % (XII)	96 % (VI)		100 % (VI)			26 % (XII)	74 % (VI)		100 % (VI)		
1.8 GPa	100 % (VI)			100 % (VI)			100 % (VI)			100 % (VI)			100 % (VI)		
1.9 GPa	100 % (VI)			100 % (VI)			100 % (VI)			100 % (VI)			100 % (VI)		

Heating rate dependence

We infer that the difference in crystallization temperatures between eHDA and VHDA above 0.3 GPa shows that the time scales of relaxation is not sufficiently short for both phases to reach the same state prior to crystallization when heating with 2 K/min. We thus lowered the heating rate to 0.5 K/min and repeated the isobaric heating at some selected pressures. Figure S2 presents the outcomes of those experiments. Generally, T_x values from slow heating experiments are several K below those from faster heating experiments at a given pressure (e.g., at 0.8 GPa $eHDA_{1.1}^{0.2}$ crystallizes at ~ 158 K heating with 0.5 K/min and at ~ 163 K heating with 2 K/min). This T_x/heating-rate dependence for a given amorphous ice is in accordance with earlier results: the higher the heating rate the higher the crystallization temperature (10-13). Qualitatively, the results concerning T_x at 0.5 K/min mirror those obtained at 2 K/min. That is, $eHDA_{1.1}^{0.2}$ crystallizes several K below $VHDA_{1.9}$ when heating with 0.5 K/min at 0.7, 0.8 and 1.8 GPa. And at small and large enough pressures (0.3 and 1.9 GPa, respectively) the T_x values approach one another. That is, for slower heating rates of 0.5 K/min the additional time available upon heating is still insufficient for VHDA and eHDA to reach the same state prior to crystallization at 0.3 GPa < p < 1.9 GPa.

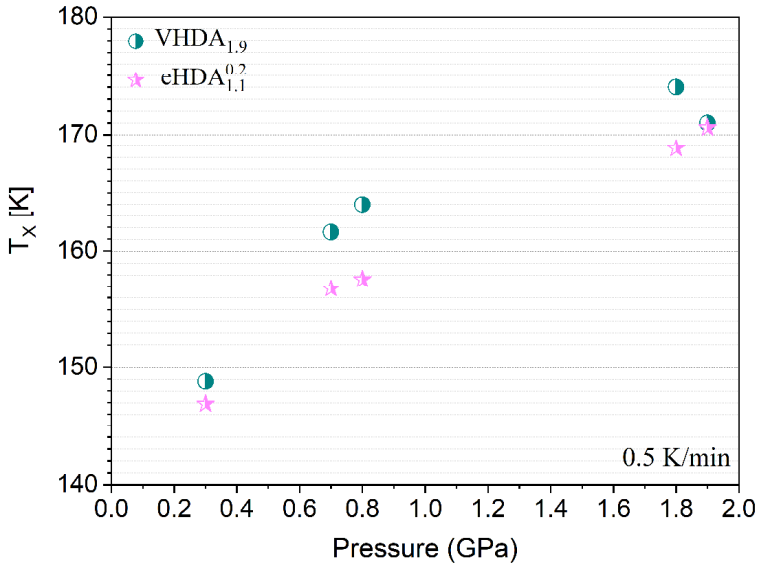

Figure S2: Crystallization temperatures from experiments at 0.5 K/min for $eHDA_{1.1}^{0.2}$ and $VHDA_{1.9}$.

Data from structural characterization of the crystallized products are displayed in Table S4. Both $eHDA_{1.1}^{0.2}$ and $VHDA_{1.9}$ transform to pure ice IX at 0.3 GPa and to pure ice VI at 1.8 and 1.9 GPa. Differences can be noted at 0.7 and 0.8 GPa. Here, $VHDA_{1.9}$ crystallizes to ice XII almost entirely (some ice IV as by-product), whereas crystallization of $eHDA_{1.1}^{0.2}$ yields amounts of ice IV equal to or even higher than amounts of ice XII, besides formation of considerable portions of ice V.

Table S4: T_x values and crystallographic data from crystallization experiments (at several pressures) of $eHDA_{1.1}^{0.2}$ and $VHDA_{1.9}$ employing a heating rate of 0.5 K/min.

	$eHDA_{1.1}^{0.2}$				$VHDA_{1.9}$		
	T_x (K)	Fraction of crystalline phases			T_x (K)	Fraction of crystalline phases	
0.3 GPa	146.9	100 % (IX)			148.8	100 % (IX)	
0.7 GPa	156.8	20 % (V)	53 % (IV)	27 % (XII)	161.6	7 % (IV)	93 % (XII)
0.8 GPa	157.6	5 % (V)	45 % (IV)	50 % (XII)	164.0	4 % (IV)	96 % (XII)
1.8 GPa	168.8	100 % (VI)			174.0	100 % (VI)	
1.9 GPa	170.6	100 % (VI)			171.0	100 % (VI)	

Crystallization rates

Crystallization rates k_x (in cm^3/s) are estimated from the initial volume of amorphous material V_{am} that is consumed in the time $t_{cryst.}$ needed for crystallization, i.e., $k_x = V_{am}/t_{cryt.}$. See Figure S5 below for the determination of t_{cryst}. Since in our experiment we directly measure uniaxial length changes rather than volume changes we also provide unidirectional crystal growth rates $k_{uni.}$ (in m/s), where we consider the height of the sample cylinder prior to crystallization h_{am}, i.e., $k_{uni.} = h_{am}/t_{cryst.}$ To determine V_{am} at a specific pressure and temperature prior to crystallization $V_{am}(T<T_x)$ we take into account the experimental sample mass (0.5 g) and the reported pressure dependence of the amorphous ices' densities just prior to crystallization $\rho(p)$ (14): for HDA (0.21 g cm^{-3} GPa^{-1}) and VHDA (0.1 g cm^{-3} GPa^{-1}), see Figure 2 in Reference (14). Knowing $V_{am}(T<T_x)$ and $t_{cryst.}$ allows one to estimate crystallization rates in cm^3/s. From the geometric constraints of the sample (cylindrical shape with a radius of 4 mm) it is possible to convert $V_{am}(T<T_x)$ into a 'sample height' $h_{am}(T<T_x)$ just prior to crystallization. Likewise, crystallization rates can then be expressed in m/s to allow for a more direct comparison with the results of Xu et al. (15). The results are displayed in Figure S3 (in tabular form in Table S5) and naturally resemble the $t_{cryst.}$ values qualitatively. The values of eHDA and VHDA match the ones reported by Handle et al. (16) to pressures up to 0.7 GPa. At $p > 0.7$ GPa however, they start to differ. While rates for eHDA and VHDA continue to drop with pressure the literature values increase above 0.7 GPa. This may be due to the fact that Handle et al. examined $eHDA_{1.1}^{0.1}$, presumably containing low-density amorphous nano-domains that transform to crystalline nano-domains upon compression (17). The crystalline seeds already present might then explain the increased crystallization rates at $p > 0.7$ GPa.

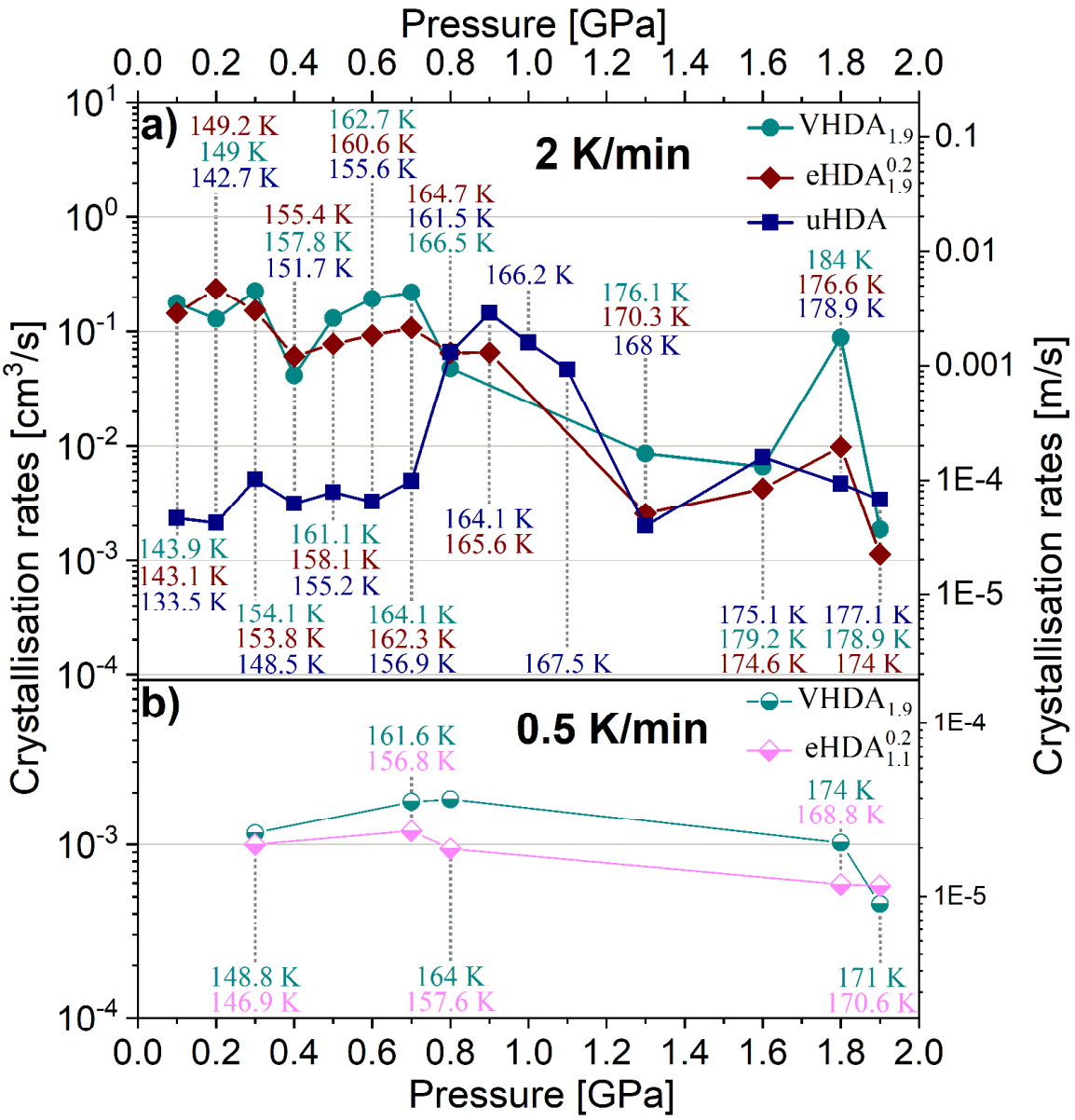

Figure S3: Crystallization rates of amorphous ices. Rates are displayed in cm^3/s (left axis) or m/s (right axis). In a) crystallization rates for $VHDA_{1.9}$ (circles), $eHDA^{0.2}_{1.9}$ (diamonds) and uHDA (squares) are shown, determined from the volume-vs.-time curves at pressures 0.1 – 1.9 GPa and a heating rate of 2 K/min. The crystallization temperatures for each pressure and amorphous ice are also presented and colour-coded correspondingly. In b) crystallization rates for $VHDA_{1.9}$ (circles) and $eHDA^{0.2}_{1.1}$ (diamonds) are shown for isobaric heating experiments with lower heating rates (0.5 K/min) at selected pressures 0.3, 0.7, 0.8, 1.8 and 1.9 GPa. The crystallization temperatures at the corresponding pressures are again colour-coded with respect to the examined amorphous ice.

Table S5: Numerical crystallization rates of amorphous ices as a function of pressure and heating rate. Rates are given in m/s and cm^3/s to allow comparison with results from different studies on the crystallization kinetics of vapor-deposited amorphous ice (15,18,19) at ambient pressure and on eHDA and VHDA at elevated pressures (16)

	2 K/min						0.5 K/min			
	$VHDA_{1.9}$		$eHDA_{1.9}^{0.2}$		uHDA		$VHDA_{1.9}$		$eHDA_{1.1}^{0.2}$	
Pressure [GPa]	crystallization rate		crystallization rate		crystallization rate		crystallization rate		crystallization rate	
	m/s	cm^3/s	m/s	cm^3/s	m/s	cm^3/s	m/s	cm^3/s	m/s	cm^3/s
0.1	$3.53 * 10^{-3}$	$1.78 * 10^{-1}$	$2.88 * 10^{-3}$	$1.45 * 10^{-1}$	–	–	–	–	–	–
0.2	$2.56 * 10^{-3}$	$1.29 * 10^{-1}$	$4.72 * 10^{-3}$	$2.37 * 10^{-1}$	–	–	–	–	–	–
0.3	$4.50 * 10^{-3}$	$2.26 * 10^{-1}$	$3.03 * 10^{-3}$	$1.52 * 10^{-1}$	–	–	$2.31 * 10^{-5}$	$1.16 * 10^{-3}$	$1.99 * 10^{-5}$	$9.99 * 10^{-4}$
0.4	$4.60 * 10^{-4}$	$2.31 * 10^{-2}$	$2.91 * 10^{-4}$	$1.47 * 10^{-2}$	–	–	–	–	–	–
0.5	$2.60 * 10^{-3}$	$1.31 * 10^{-1}$	$1.55 * 10^{-3}$	$7.79 * 10^{-2}$	–	–	–	–	–	–
0.6	$3.84 * 10^{-3}$	$1.93 * 10^{-1}$	$1.84 * 10^{-3}$	$9.25 * 10^{-2}$	$6.38 * 10^{-5}$	$3.21 * 10^{-3}$	–	–	–	–
0.7	$4.37 * 10^{-3}$	$2.20 * 10^{-1}$	$2.13 * 10^{-3}$	$1.07 * 10^{-1}$	$9.14 * 10^{-5}$	$4.59 * 10^{-3}$	$3.54 * 10^{-5}$	$1.78 * 10^{-3}$	$2.18 * 10^{-5}$	$1.20 * 10^{-3}$
0.8	$9.57 * 10^{-4}$	$4.81 * 10^{-2}$	$1.30 * 10^{-3}$	$6.53 * 10^{-2}$	$1.29 * 10^{-3}$	$6.49 * 10^{-2}$	$3.65 * 10^{-5}$	$1.84 * 10^{-3}$	$1.83 * 10^{-5}$	$9.47 * 10^{-4}$
0.9	–	–	$1.30 * 10^{-3}$	$6.54 * 10^{-2}$	$2.84 * 10^{-3}$	$1.47 * 10^{-1}$	–	–	–	–
1.0	–	–	–	–	$1.57 * 10^{-3}$	$7.88 * 10^{-2}$	–	–	–	–
1.1	–	–	–	–	$9.16 * 10^{-4}$	$4.61 * 10^{-2}$	–	–	–	–
1.3	$1.70 * 10^{-4}$	$8.57 * 10^{-3}$	$5.09 * 10^{-5}$	$2.56 * 10^{-3}$	$3.92 * 10^{-5}$	$1.97 * 10^{-3}$	–	–	–	–
1.6	$1.31 * 10^{-4}$	$6.60 * 10^{-3}$	$8.44 * 10^{-5}$	$4.24 * 10^{-3}$	$1.57 * 10^{-4}$	$7.88 * 10^{-3}$	–	–	–	–
1.8	$1.76 * 10^{-3}$	$8.84 * 10^{-2}$	$1.95 * 10^{-4}$	$9.78 * 10^{-3}$	$9.21 * 10^{-5}$	$4.63 * 10^{-3}$	$2.03 * 10^{-5}$	$1.02 * 10^{-4}$	$1.14 * 10^{-5}$	$5.89 * 10^{-4}$
1.9	$3.69 * 10^{-5}$	$1.86 * 10^{-3}$	$2.24 * 10^{-5}$	$1.13 * 10^{-3}$	$6.70 * 10^{-5}$	$3.37 * 10^{-3}$	$9.05 * 10^{-6}$	$4.55 * 10^{-4}$	$1.12 * 10^{-5}$	$5.78 * 10^{-4}$

Determination of crystallization temperature T_x under pressure and structural characterization by powder XRD

The final state of the amorphous ices can be preserved by quenching with liquid N_2 to ~ 80 K. At ~80 K the samples are subsequently brought to the target pressure and then heated isobarically with 2 K/min beyond crystallization. Upon crystallization a volumetric change occurs due to the difference in density between the amorphous state prior to and the ice polymorphs after crystallization. Figure S4 a) exemplifies how to extract the crystallization temperature T_x from the volume curves recorded in isobaric heating experiments for the five amorphous ices at 1.9 GPa. Upon heating the samples may initially either exhibit expansion (as is the case here for $VHDA_{1.9}$) or densification (as for all other amorphous ices here). In this case expansion prior to crystallization is likely elastic, whereas densification implies relaxation of the amorphous material to a denser state. When the amorphous samples transform to crystalline phase mixtures, a rather sudden and abrupt volume change occurs. Depending on the density difference between crystalline and amorphous state, the crystallization may either be associated with an abrupt expansion or densification. In the example of Figure S4 a) all amorphous states in fact densify and transform to pure ice VI, which has a higher density than all amorphous ices at 1.9 GPa. We define the onset temperature of crystallization T_x by the intersection of two tangents in the volume curve just prior to and during the transformation (see dark grey solid lines in Figure S4 a)). This is found at T = 174 – 179 K in the example of Figure S4 a) (see dotted lines). When the crystallization is complete the samples are quenched with liquid N_2 and recovered to ambient pressure. Figure S4 b) exhibits exemplary diffractograms of quench-recovered samples obtained after isobaric heating at 1.9 GPa (see Figure S4 a)). They demonstrate that in all cases crystallization at 1.9 GPa results in the formation of pure ice VI. At other pressures phase mixtures of up to four different polymorphs were observed. In these cases the most intense Bragg peaks (100 % relative intensity, see Table S1) of the individual polymorphs were compared to estimate the relative abundances of crystalline phases in a mixture.

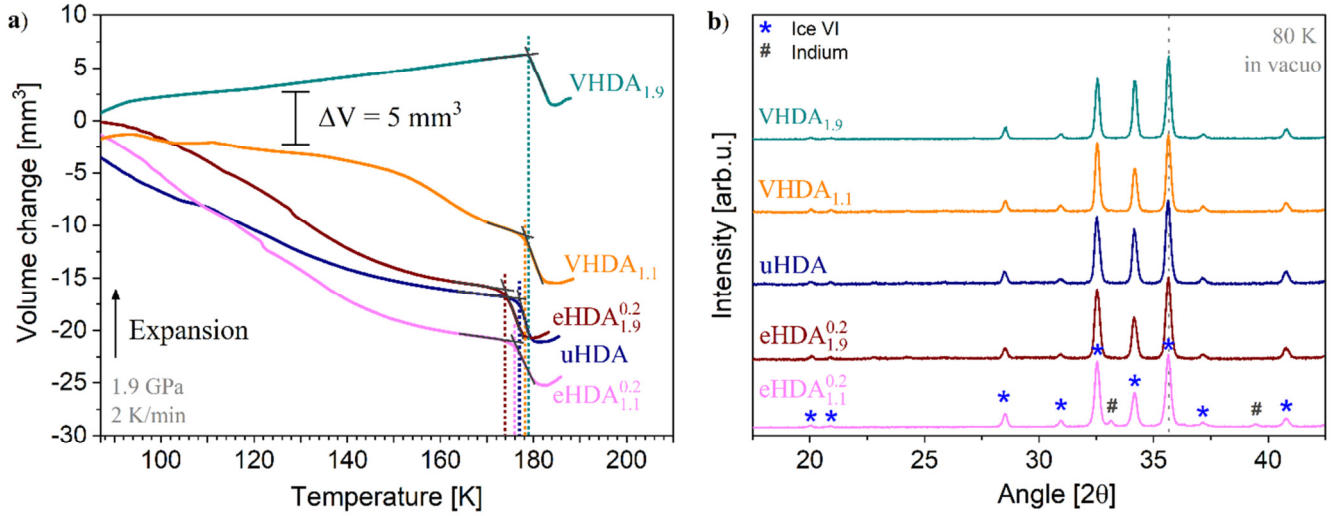

Figure S4: a) Volume curves from isobaric heating experiments at 1.9 GPa, 2 K/min. Dotted lines indicate the onset of T_x of the amorphous ices, dark grey lines represent tangents by which T_x is defined. b) Powder X-ray diffraction patterns of samples crystallized at 1.9 GPa, recorded at ~ 80 K and ~ $5 \cdot 10^{-1}$ mbar. The asterisks mark the positions of the ice VI Bragg peaks. The grey dotted line marks the position of the most intense (100 %) Bragg peak of ice VI. The pound signs mark the positions of indium Bragg peaks.

Determination of crystallization times t_{cryst} under pressure

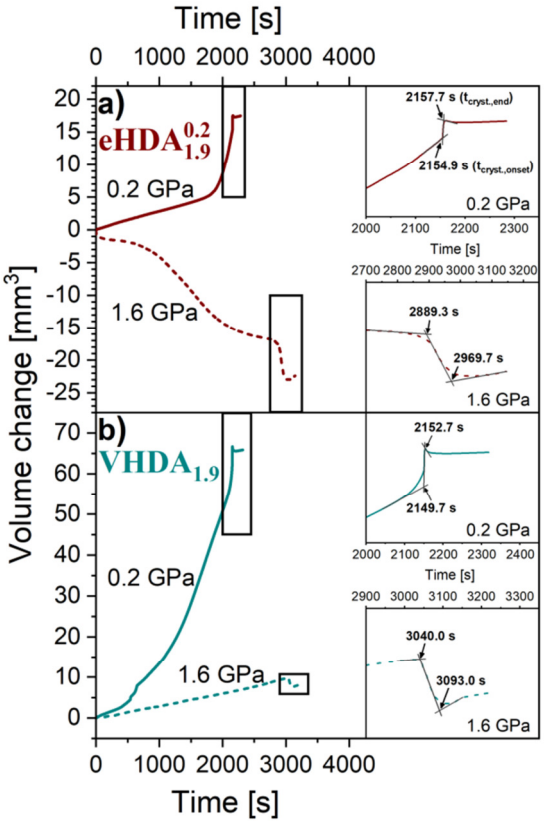

Figure S5: Determination of crystallization times of a) $eHDA^{0.2}_{1.9}$ and b) $VHDA_{1.9}$ at 0.2 GPa (solid lines) and 1.6 GPa (dashed lines). Insets represent magnifications of the rectangles. Onset and offset times are determined from the tangent intersections as shown in the insets.

Analogous to the definition of onset/offset *temperatures* of crystallization one can then define onset/offset *times* of crystallization by analysing the volume curves as a function of time, see Figure S5. That is, a time frame in which crystallization occurs at a given pressure for a given amorphous ice. It has to be pointed out that on the basis of our data it is not possible to differentiate between crystal nucleation and growth processes. Thus, we want to stress that our results reflect the bulk crystallization as a whole. It has been shown in previous studies that samples quench-recovered just prior to the step-like change in volume show only minor amounts of crystalline material in an amorphous matrix, as determined by structural characterization (powder XRD) (8,9,12,20). The step in the volume-vs.-temperature (or volume-vs.-time) curve can hence be attributed to crystallization of the sample rather than volume change in the amorphous matrix. This requires well separated time scales of relaxation and crystallization, which was recently demonstrated by us (16).

References

1. Dowell LG & Rinfret AP (1960) Low temperature forms of ice as studied by X-ray diffraction. *Nature* 188:1144-1148.
2. Kamb B (1964) Ice II: a proton-ordered form of ice. *Acta Crystallogr.* 17(11):1437-1449.
3. Engelhardt H & Kamb B (1981) Structure of ice IV, a metastable high-pressure phase. *J. Chem. Phys.* 75:5887-5899.
4. Kamb B, Prakash A, & Knobler C (1967) Structure of ice V. *Acta Cryst.* 22:706-715.
5. Kamb B (1965) Structure of ice VI. *Science* 150:205-209.
6. Lobban C, Finney JL, & Kuhs WF (2000) The structure and ordering of ices III and V. *J. Chem. Phys.* 112:7169-7180.
7. Koza M, Schober H, Tölle A, Fujara F, & Hansen T (1999) Formation of ice XII at different conditions. *Nature* 397:660-661.
8. Seidl M, Amann-Winkel K, Handle PH, Zifferer G, & Loerting T (2013) From parallel to single crystallization kinetics in high-density amorphous ice. *Physical Review B* 88(17):174105.
9. Seidl M, Fayter A, Stern JN, Zifferer G, & Loerting T (2015) Shrinking water's no man's land by lifting its low-temperature boundary. *Physical Review B* 91(14):144201.
10. Salzmann CG, Mayer E, & Hallbrucker A (2004) Effect of heating rate and pressure on the crystallization kinetics of high-density amorphous ice on isobaric heating between 0.2 and 1.9 GPa. *Phys. Chem. Chem. Phys.* 6(22):5156-5165.
11. Salzmann CG, Kohl I, Loerting T, Mayer E, & Hallbrucker A (2003) Pure ices IV and XII from high-density amorphous ice. *Can. J. Phys.* 81:25-32.
12. Stern J & Loerting T (2017) Crystallization of the amorphous ices in the intermediate pressure regime. *Scientific Reports* 7(1):3995.
13. Stern JN & Loerting T (2018) On the crystallization temperature of very high-density amorphous ice. *Physical Chemistry Chemical Physics*.
14. Salzmann CG*, et al.* (2006) Isobaric annealing of high-density amorphous ice between 0.3 and 1.9 GPa: in situ density values and structural changes. *Phys. Chem. Chem. Phys.* 8:386-397.
15. Xu Y, Petrik NG, Smith RS, Kay BD, & Kimmel GA (2016) Growth rate of crystalline ice and the diffusivity of supercooled water from 126 to 262 K. *Proc. Natl. Acad. Sci. U. S. A.* 113(52):14921-14925.
16. Handle PH & Loerting T (2016) Dynamics anomaly in high-density amorphous ice between 0.7 and 1.1 GPa. *Physical Review B* 93(6):064204.
17. Tonauer CM, Seidl-Nigsch M, & Loerting T (2018) High-density amorphous ice: nucleation of nanosized low-density amorphous ice. *J. Phys.: Condens. Matter* 30(3):034002.
18. Hage W, Hallbrucker A, Mayer E, & Johari GP (1994) Crystallization kinetics of water below 150 K. *J. Chem. Phys.* 100:2743-2747.
19. Jenniskens P & Blake DF (1996) Crystallization of amorphous water ice in the Solar System. *Astrophy. J.* 473(2, Pt. 1):1104-1113, 1101 plate.
20. Handle PH & Loerting T (2018) Experimental study of the polyamorphism of water. II. The isobaric transitions between HDA and VHDA at intermediate and high pressures. J Chem Phys 148(12):124509